Technical Note

Comparison of Phase-Difference and Complex-Difference Processing in Phase-Contrast MR Angiography[1]

Matt A. Bernstein, PhD • Yoshikazu Ikezaki, MS

The two main phase-contrast reconstruction methods are phase difference and complex difference. The signal-to-noise ratio properties and relative advantages of the two techniques are discussed. It is argued that each processing method has applications in which it is superior, and guidelines are provided to determine those applications. It is demonstrated theoretically and experimentally that only the complex-difference method is well suited for processing phase-contrast slabs with use of a projection dephaser gradient.

Index terms: Image processing • Magnetic resonance (MR), angiography • Phase-contrast imaging • Physics • Reconstruction algorithms

JMRI 1991; 1:725–729

[1] From the Applied Science Laboratory, GE Medical Systems, 3200 N Grandview Blvd, Waukesha, WI 53188 (M.A.B.); and Yokogawa Medical Systems, Tokyo (Y.I.). Received June 21, 1991; revision requested August 5; revision received August 19; accepted August 20. **Address reprint requests to** M.A.B.

PHASE-CONTRAST IMAGES are acquired by collecting multiple magnetic resonance (MR) imaging data sets with different values of the first gradient moment. We call the acquisition of a single data set with a specific first moment a "flow experiment." To obtain the desired vascular image representing flow along a single direction, subtraction is performed on a pair of flow experiments with different first gradient moments along that direction. Because the first gradient moment affects only the phase of moving spins, the subtraction suppresses signal from stationary tissue. Two methods of performing this subtraction have been described in the literature: phase difference (1–3) and complex difference (4). The phase-difference method forms arctangent images from each flow experiment and then subtracts the images on a pixel-by-pixel basis. The resulting phase-difference image can then be multiplied by a magnitude image (or thresholded by some alternative technique) to reduce the image background noise due to air.

In the second method of subtraction, the complex-difference approach, subtraction of the raw data sets obtained from two flow experiments is followed by a standard magnitude reconstruction. (The subtraction can equivalently be performed after inverse Fourier transformation but before the magnitude operation.)

This report compares the relative advantages of phase-difference and complex-difference processing. Signal-to-noise ratios (S/Ns) are calculated, and suitability of these techniques for processing thick-slab two-dimensional (2D) acquisitions is discussed.

Finally, there is a third acquisition-reconstruction scheme (5). That scheme acquires data from three flow experiments to determine flow along a single gradient axis and retains the advantages of the complex-difference method for processing thick slabs and the quantitative aspect of the phase-difference method. That method is beyond the scope of this report and is mentioned only for completeness.

• SIMPLIFIED S/N CONSIDERATIONS IN THE ABSENCE OF STATIONARY TISSUE

Phase-Difference Methods

Consider a simplified phase-difference flow experiment, as shown in Figure 1. This experiment assumes that there is no contribution from stationary tissue within the voxel of interest (that complication is treated in the next section). First, consider a single flow measurement. The flow measurement can be described by a complex number Z that has real and imaginary components I and Q, respectively, or alternatively polar coordinates M and θ, respectively. Figure 1 shows a pair of flow measurements labeled *1* and *2*. (The figures and analysis assume that the data have already been Fourier transformed into the image domain.) For convenience, and without loss of generality, we choose zero phase (I axis) to be the average of the two phases. Let $I_1 = I_2 = I$, $|Q_1| = |Q_2| = Q$, $|\theta_1| = |\theta_2| = \theta$, $M_1 = M_2 = M$, and $2\theta = \Delta\theta$. The complex-difference image displays $2|Q|$ on a pixel-by-pixel basis, while the phase-difference image displays $\Delta\theta$. Suppose that I and Q are independent measurements, each with variance σ^2. Then (6,7) the variance in θ is

$$\sigma_\theta^2 = (\partial\theta/\partial I)^2\sigma_I^2 + (\partial\theta/\partial Q)^2\sigma_Q^2, \quad (1)$$

with $\sigma_I = \sigma_Q = \sigma$.

Since $\theta = \tan^{-1}(Q/I)$ and $M^2 = I^2 + Q^2$, the derivatives can be evaluated to give

$$\sigma_\theta = \sigma/M. \quad (2)$$

Note that the variance in θ goes to infinity as M goes to zero. For example, M is equal to zero in the air background.

Although this divergence is mathematically true, recall that in practice (due to the representation of the arctangent function) phase measurements are limited to the range $-\pi$ to π. Therefore, true variance in a phase image is always finite, even when M is equal to zero.

Often phase images are masked by multiplication with the magnitude image to suppress the meaningless (but noisy) phase values in low-M regions of the image (7). The high pixel values from the air background in an unmasked phase image are visually distracting and virtually preclude postprocessing methods such as maximum-intensity projection (MIP) because the noise background in air has the same dynamic range as the desired signal. By suppressing the noise with a multiplicative magnitude mask to form the product $M\theta$, the appearance of the flow image is greatly improved. In such cases, the quantity $\sigma_{M\theta}$ is of more interest than σ_θ. Because M is also a function of I and Q, the variance $\sigma^2_{M\theta}$ of the magnitude-weighted phase image is *not* simply $M\sigma_\theta = \sigma$. Instead this variance is given by

$$\sigma^2_{M\theta} = \sigma^2(1 + \theta^2)$$
$$= \sigma^2[1 + (\Delta\theta/2)^2]. \quad (3)$$

Next we calculate the variance for a magnitude-masked phase-difference flow experiment. With most acquisition schemes, we use an averaged magnitude mask:

$$A = (|Z_1| + |Z_2|)/2 = M. \quad (4)$$

With a development similar to Equation (1), the variance $\sigma^2_{A\Delta\theta}$ can be calculated:

$$\sigma^2_{A\Delta\theta} = [\partial(A\Delta\theta)/\partial\Delta\theta]^2\sigma^2_{\Delta\theta} + [\partial(A\Delta\theta)/\partial A]^2\sigma^2_A$$
$$= A^2\sigma^2_{\Delta\theta} + \Delta\theta^2\sigma^2_A. \quad (5)$$

Because the flow experiments *1* and *2* are uncorrelated, the variance $\sigma^2_{\Delta\theta}$ is twice σ^2_θ, or $\sigma^2_{\Delta\theta} = 2\sigma^2/M^2 = 2\sigma^2/A^2$. The averaged mask A is used to improve S/N; that is, although A is equal to M, its variance is less: $\sigma^2_A = \sigma^2_M/2 = \sigma^2/2$. Substituting these results into Equation (5), we obtain the desired variance:

$$\sigma^2_{A\Delta\theta} = 2\sigma^2 + (\Delta\theta)^2\sigma^2/2$$
$$= 2\sigma^2[1 + (\Delta\theta/2)^2], \quad (6)$$

while the signal $A\Delta\theta$ is equal to $M\Delta\theta$. Therefore, the S/N in a magnitude-weighted phase-difference image is given by

$$(S/N)_{A\Delta\theta} = \frac{\sqrt{2}\,M\,(\Delta\theta/2)}{\sigma\sqrt{1 + (\Delta\theta/2)^2}}, \quad (7)$$

for $-\pi < \Delta\theta < \pi$. Note that the detailed form of Equation (7) depends on the number of flow experiments used to construct the averaged magnitude mask. We have used two here, but the S/N can be similarly derived for other common choices such as one, four, or six experiments.

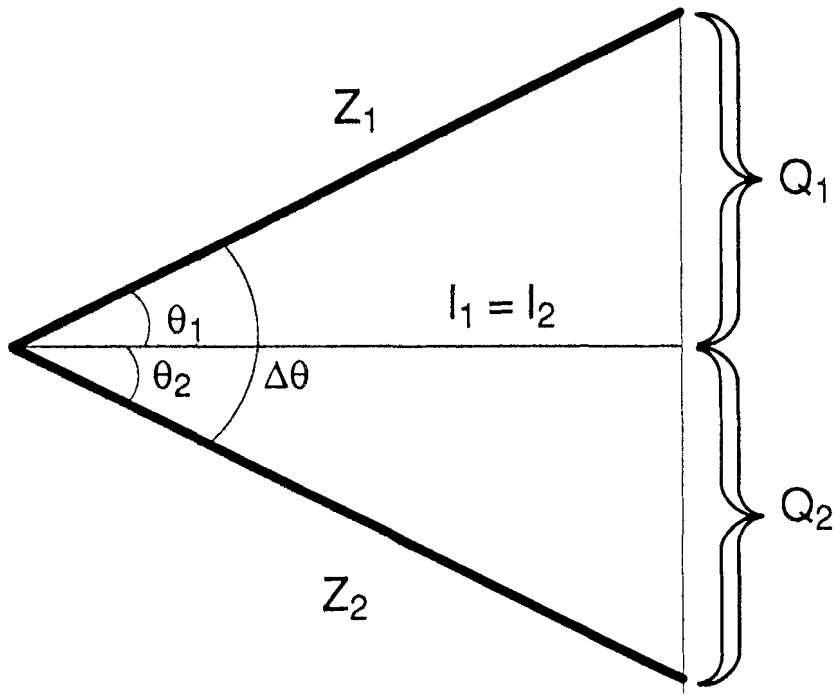

Figure 1. Pair of flow measurements (bold lines) characterized by polar coordinates $M = |Z_1| = |Z_2|$ and θ or rectangular coordinates I and Q. The variance in the I and Q measurements is σ^2 for each.

Complex-Difference Methods

Next, we can analyze the noise in the complex-difference image. Referring to Figure 1, let Z_1 be a complex data point (again, after the inverse Fourier transformation) $Z_1 = I_1 + iQ_1$, and similarly for Z_2. The complex-difference image is formed by calculating, on a pixel-by-pixel basis,

$$\Delta Z = |Z_1 - Z_2|. \quad (8)$$

For the case shown in Figure 1, the complex-difference image is simply $2|Q| = 2M|\sin(\Delta\theta/2)|$. The variance in the complex-difference measurement is given by

$$\sigma^2_{\Delta Z} = 2\sigma^2, \quad (9)$$

which is independent of both M and $\Delta\theta$. (As described in reference 8 and references therein, Equation [9] is an approximation that is highly accurate when S/N exceeds 2.) The S/N for the complex-difference image is

$$(S/N)_{\Delta Z} = \frac{\sqrt{2}\,M|\sin(\Delta\theta/2)|}{\sigma}, \quad (10)$$

for $-\pi < \Delta\theta < \pi$. Note from Equations (6) and (9) that $\sigma^2_{A\Delta\theta}$ is greater than or equal to $\sigma^2_{\Delta Z}$ for all values of $\Delta\theta$. That is, the complex-difference image is inherently less noisy than the phase-difference image. As will be seen in the next subsection, however, this noise statistic is misleading in some cases.

Signal and S/N of the Two Methods

The S/N characteristics of each method as described by Equations (7) and (10) are summarized graphically in Figure 2 (see the curves labeled *Complex Difference* and *Phase Difference [1]*). Over the range $-\pi < \Delta\theta < \pi$, the complex-difference method has a small S/N advantage. The phase-difference method has a dynamic range advantage because it can distinguish directional flow by means of signed pixel values. The dynamic range advantage is lost, however, when a "speed," or sum-of-squares, image is calculated from three signed (directional) flow images.

Even on single-flow-direction images, the dynamic range of the complex-difference method can be made equal to that of the phase-difference method. One method for accomplishing this is to use the sign of the phase-difference image as a multiplicative mask for the complex-difference image (Nishimura DG, private oral communication, 1991). Several interesting effects occur, since the noise in the phase-difference image $\sigma^2_{A\Delta\theta}$ (Eq [6]) depends on $\Delta\theta$. For example, in magnitude-masked phase-difference images, the air background (with its random $\Delta\theta$) appears noisier than the stationary tissue background ($\Delta\theta$ near zero).

As mentioned, the vessel S/N alone can be a misleading measure for pre-

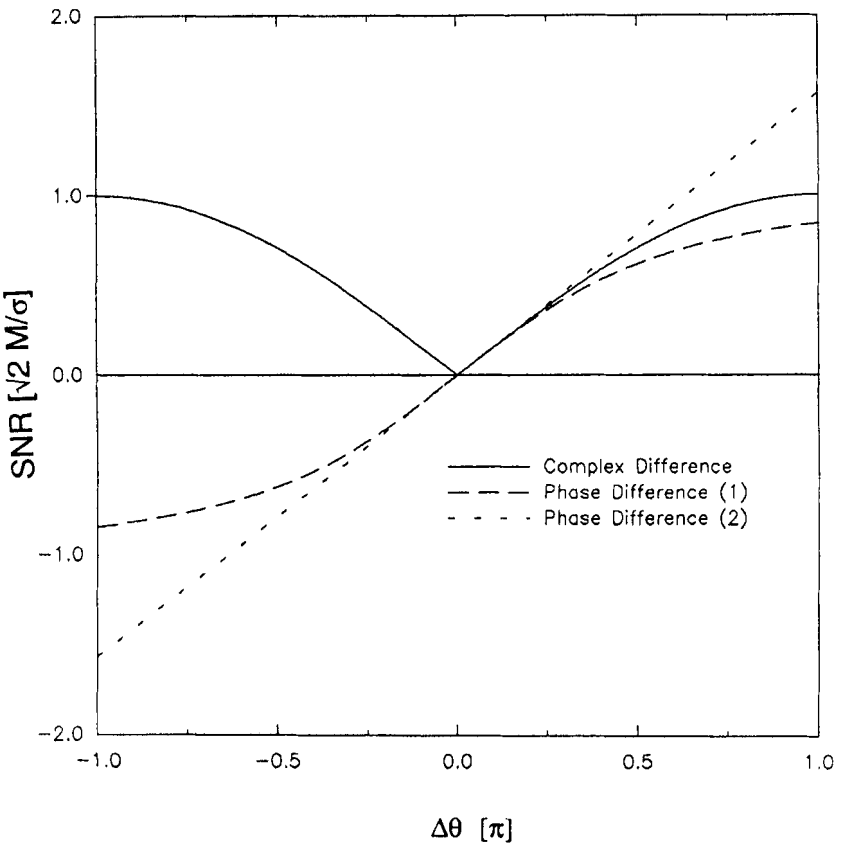

Figure 2. S/N (*SNR*) versus $\Delta\theta$ in the absence of stationary tissue. The S/Ns for the phase-difference and complex-difference methods are given by Equations (7) and (10), respectively. *Phase Difference (1)* reflects the $\Delta\theta$ dependence of the noise and models the S/N within vessels. *Phase Difference (2)* uses the noise from stationary tissue ($\Delta\theta = 0$) and models the vessel-to-background S/N. Both the phase-difference and complex-difference methods undergo flow-related aliasing when $|\Delta\theta|$ is greater than π.

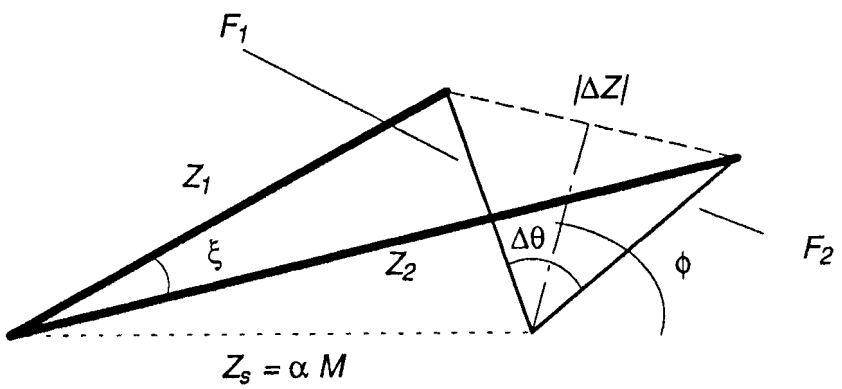

Figure 3. Pair of complex flow measurements Z_1 and Z_2 (bold lines) in the presence of a stationary tissue contribution Z_s (dotted line). The complex difference $|\Delta Z|$ (dashed line) is independent of the stationary tissue contribution. This is in distinction to the magnitude masked phase difference $\xi(|Z_1| + |Z_2|)/2$, which can depend strongly on the stationary tissue contribution. Note that this figure reduces to the equivalent of Figure 1 when Z_s is equal to zero.

dicting the detectability of small vessels in a phase-difference image. This effect arises from the $\Delta\theta$ dependence in $\sigma^2_{A\Delta\theta}$. The detectability problem we usually encounter is distinguishing a small vessel embedded in a stationary tissue background. In the phase-difference image, the noise in the stationary tissue (where $\Delta\theta = 0$) is less than in the vessel itself. The curve labeled *Phase Difference (2)* in Figure 2 shows the S/N for the phase-difference method, with the noise now calculated for the stationary tissue background. From this point of view, the phase-difference method has a slight advantage over the complex-difference method.

The conclusion drawn from the S/N analysis, therefore, is that the S/N in the vessels is slightly better with the complex-difference method, while the signal-to-*background* noise, a determinant of detectability, is somewhat better with the phase-difference method.

Experimental Test of the S/N Calculation

According to Equations (7) and (10), when $\Delta\theta$ is equal to π the S/Ns of images processed with the complex-difference and phase-difference methods should differ. This prediction was tested experimentally. A rotating disk phantom (9) driven by a direct-current motor (model MH2630-101A; Torque Systems, Watertown, Mass) at 29.5 rpm ± 0.2 was imaged with a Signa 1.5-T imager (GE Medical Systems, Milwaukee). S/N measurements were made at a radial distance of 8.1 cm (where $\Delta\theta = \pi$, in accordance with the peak-velocity encoding [VENC = 25 cm/sec]). An absolute-value version of the masked phase-difference image was used to avoid sign fluctuations near $\Delta\theta = \pi$. Based on 10 1.13 × 0.23-cm regions of interest (each containing 120 pixels), the S/N results were 0.997 ± 0.007 and 0.849 ± 0.064 (in units of $\sqrt{2}\,M/\sigma$) for complex- and phase-difference processing, respectively. This is in good agreement with the predicted values of 1.00 and 0.844. The larger error in the phase-difference S/N measurement is believed to result from its sensitivity to correlated contributions (radio-frequency penetration, etc) to σ in the magnitude image.

• EFFECTS OF STATIONARY AND FLOWING TISSUES IN THE SAME VOXEL

Images processed with the phase-difference method are degraded when stationary tissue contributes to the voxel of interest. In contrast, images processed with the complex-difference method are independent of stationary tissue. In this section, the effect of stationary tissue on the signal generated with the phase-difference method is calculated.

We adopted a simplified model for the contribution of stationary tissue. Stationary tissue (dotted line in Fig 3) is assumed (without loss of generality) to be real and to have an adjustable signal strength

$$Z_S = \alpha M, \qquad (11)$$

where M is the magnitude of the com-

plex flow measurements F_1 and F_2. When the scalar parameter α is equal to zero, there is no stationary tissue contribution and the analysis reduces to that shown in the previous section. The scalar parameter α is therefore a means by which to selectively include stationary tissue effects. As shown in Figure 3, ϕ is defined as the phase angle between the stationary tissue signal and the bisector of the flow measurements, or

$$\phi = \arg (F_1 + F_2). \quad (12)$$

The physical interpretation of the phase angle ϕ is discussed in the next section. The parameter ϕ is important because the signal obtained with the phase-difference method depends on it. Let Figure 3 schematically show the flow measurements after inverse Fourier transformation. Then,

$$Z_1 = Z_S + F_1 = \alpha M + Me^{i(\phi+\theta)}, \quad (13)$$

with $\theta = \Delta\theta/2$,

$$Z_2 = Z_S + F_2 = \alpha M + Me^{i(\phi-\theta)}, \quad (14)$$

with $\theta = \Delta\theta/2$,

$$\begin{aligned} \xi &= \arg (Z_1/Z_2) \\ &= \arg (Z_1Z_2^*/|Z_2|^2) \\ &= \arg (Z_1Z_2^*). \end{aligned} \quad (15)$$

With most acquisition schemes, we use the averaged magnitude mask A given by Equation (4). With the averaged magnitude mask, the signal as a function of α, θ, $\Delta\theta = 2\theta$, and ϕ is

$$\begin{aligned} S &= \xi(|Z_1| + |Z_2|)/2 \\ &= M/2\,[\sqrt{1 + \alpha^2 + 2\alpha\cos(\phi + \theta)} \\ &\quad + \sqrt{1 + \alpha^2 + 2\alpha\cos(\phi - \theta)}] \\ &\quad \times \tan^{-1} \left(\frac{\sin\Delta\theta + 2\alpha\sin\theta\cos\phi}{\cos\Delta\theta + \alpha^2 + 2\alpha\cos\theta\cos\phi} \right). \end{aligned} \quad (16)$$

Figure 4 shows this signal plotted versus ϕ for various stationary tissue contributions α and for $\Delta\theta = \pi/2$. At $\alpha = 0$, the signal is independent of ϕ, as expected. As α increases, the signal has a stronger dependence on ϕ. The point to emphasize here is that regions of zero signal, or dropouts, can be produced with phase-difference processing when there is a considerable stationary tissue contribution to the voxel of interest and the angle ϕ varies. Note from Equations (8), (13), and (14), as well as Figure 3, that the complex difference ΔZ (unlike the phase difference) is independent of Z_s and hence independent of the angle ϕ.

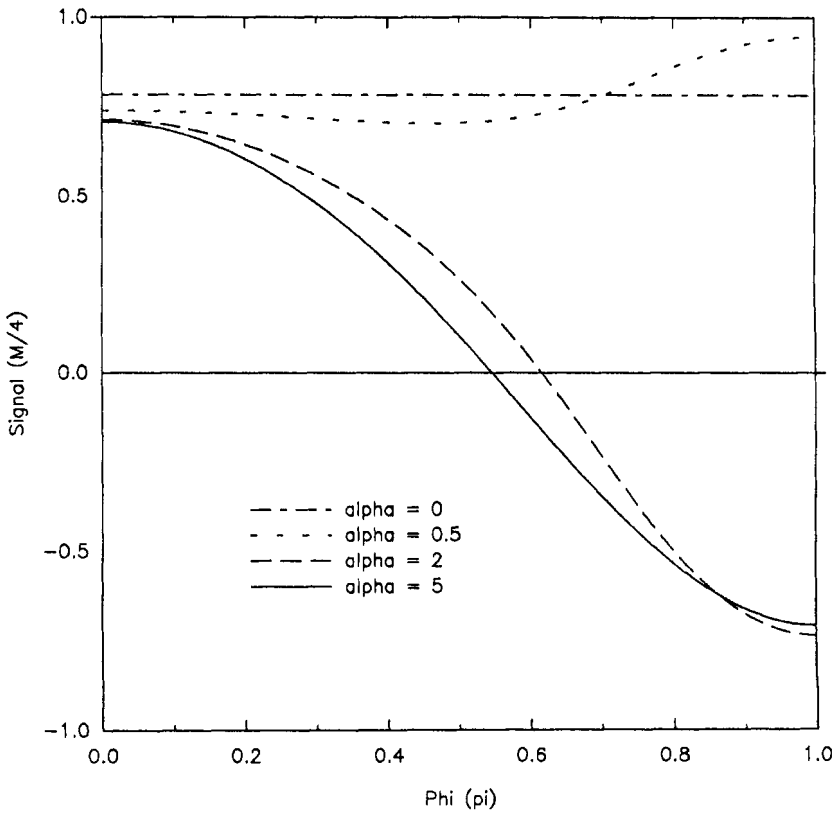

Figure 4. Signal versus phase difference in the presence of stationary tissue, calculated from Equation (16) ($\Delta\theta$ is set to $\pi/2$). The stationary tissue contribution increases with α. Note the artifactual sign reversals for $\alpha = 2$ and $\alpha = 5$.

• PITTING ARTIFACTS AND SIGN REVERSALS

For thick slabs processed with phase-difference methods, a "pitting" artifact can sometimes be seen. Examples of such artifacts in the basilar artery near the circle of Willis are shown in Figure 5b. Such artifacts are not seen in the corresponding image reconstructed with the complex-difference method (Fig 5a). The origin of this effect is suggested by Figure 3. The pitting artifact occurs where the angle ξ goes to zero, which can occur only at specific values of ϕ. Figure 4 further illustrates this.

The angle ϕ varies within 2D phase-contrast images primarily because of the projection dephaser gradient (10) used. The projection dephaser is used only on thick-slab 2D phase-contrast acquisitions. It is implemented with a gradient of nonzero area for section selection and refocusing and acts as a high-pass spatial filter to improve stationary tissue suppression. The net surviving stationary tissue signal after the projection dephaser has some phase, which we have set to zero (again, without loss of generality) in Figure 3. If the projection dephaser is implemented with the section-select gradient, the coordinate of the vessel along the section-select direction will determine ϕ. The images in Figure 5 have a projection dephaser gradient strength such that a 2π phase wrap is produced every 15 mm.

The artifactual zero crossings (ie, $\xi = 0$) are the cause of the pitting artifact seen in Figure 5b and are accompanied by spurious sign reversals in images in which flow direction is encoded in the pixel sign. Although pitting is apparent on sum-of-square images (Fig 5b), the artifactual sign reversals are not.

• CONCLUSION

The phase-difference and complex-difference methods are the two in common use for reconstructing phase-contrast data. Advantages of the phase-difference method include ability to provide (*a*) quantitative results because velocity is directly proportional to phase shift θ and (*b*) optimal detectability of small vessels against a background of stationary tissue. The drawback of the phase-difference method is pitting artifact when the method is implemented in conjunction with projection dephaser gradients or any other acquisition scheme that leads to variations in the angle ϕ shown in Figure 3. (For example, if dynamic range compression were accomplished by means of a nonlinear phase radio-frequency pulse [11] instead of the projection dephaser gradient, we expect that the

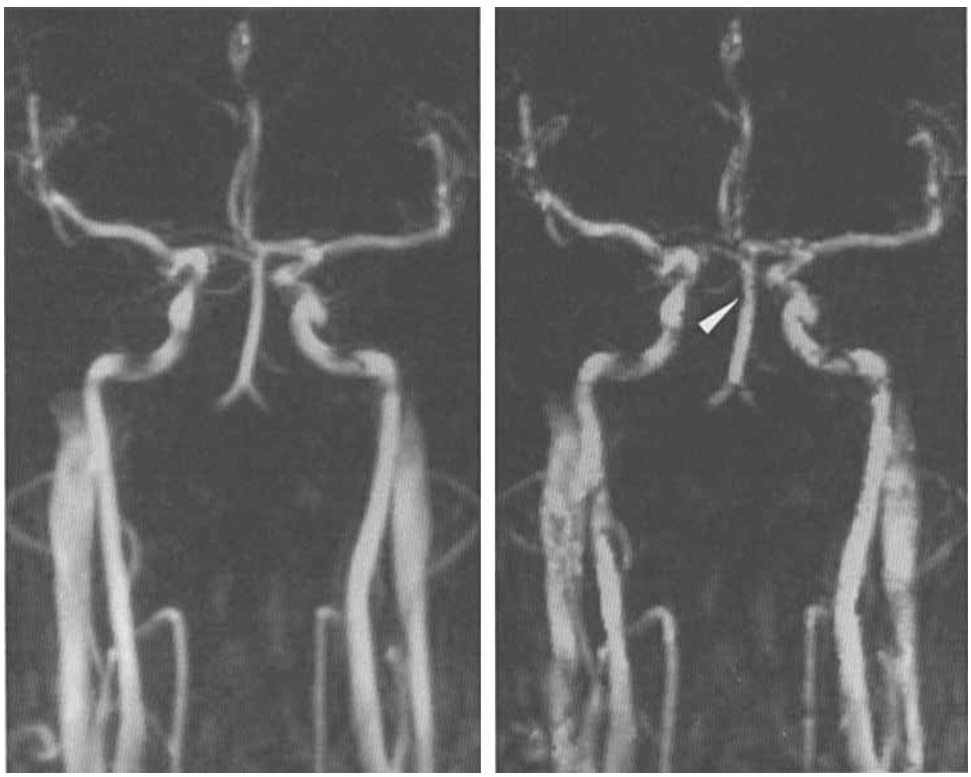

a. **b.**

Figure 5. Comparison of complex-difference (**a**) and phase-difference (**b**) processing of the same raw data. Phase-difference processing is not optimal in conjunction with the projection dephaser gradient, as indicated by the pitting artifact seen in **b** (arrowhead). These are sum-of-square images sensitive to flow in all three directions. Acquisition parameters: slab thickness = 50 mm, 192 × 256 matrix, eight signals averaged, 20-cm field of view, TR = 33 msec, TE = 7.8 msec, flip angle = 20°, peak velocity encoding = 40 cm/sec, acquisition time = 3 minutes 25 seconds.

artifact would persist.) As mentioned, the variations in ϕ lead to poor image quality for thick-slab 2D images. Because sign reversals accompany zero crossings, we demonstrated the simple rule that a *phase-difference image that has the pitting artifact described herein will yield unreliable directional flow information.* Our experience has been that without the projection dephaser gradient, no pitting artifact is seen with phase-difference processing, although stationary tissue suppression for sections thicker than approximately 20 mm is degraded.

The pitting artifact should not be confused with other signal voids that are commonly seen on MR angiograms and that are due to complicated flow patterns (turbulence, flow separations, etc). The use of complex-difference processing will remove the pitting artifact described here but will not remove other signal voids.

The strengths of the complex-difference method are (*a*) compatibility with projection dephaser gradients, thereby optimizing image quality in thick-slab 2D acquisitions, and (*b*) optimal S/N within the vessels. ●

Acknowledgments: Technical assistance from Kirk Udovich, BS, who wrote the reconstruction programs, is highly appreciated. Helpful discussions with Eiji Yoshitome, PhD, Norbert Pelc, ScD, David Weber, PhD, Frank Korosec, PhD, Steven Souza, PhD, Charles Dumoulin, PhD, and Chao Tang, MS, are acknowledged.

References

1. Bryant DJ, Payne JA, Firmin DN, Longmore DB. Measurement of flow with NMR imaging using a gradient pulse and phase difference technique. J Comput Assist Tomogr 1984; 8:588–593.
2. Nayler GL, Firmin DN, Longmore DB. Blood flow imaging by cine magnetic resonance. J Comput Assist Tomogr 1986; 10:715–722.
3. Spritzer CE, Pelc NJ, Lee JN, Evans AJ, Sostman HD, Riederer SJ. Rapid MR imaging of blood flow with a phase-sensitive, limited-flip-angle gradient recalled pulse sequence: preliminary experience. Radiology 1990; 176:255–262.
4. Dumoulin CL, Souza SP, Walker MF, Wagle W. Three dimensional phase contrast angiography. Magn Reson Med 1989; 9:139–149.
5. Ikezaki Y, Yoshitome E. MRA which indicates velocity using phase contrast method. Jpn J MR Med 1990; 10:346.
6. Conturo TE, Smith GD. SNR in phase angle reconstruction: dynamic range extension using phase reference offsets. Magn Reson Med 1990; 15:420–437.
7. Pelc NJ, Bernstein MA, Shimakawa A, Glover GH. Encoding strategies for three-direction phase-contrast MR imaging of flow. JMRI 1991; 1:405–413.
8. Bernstein MA, Thomasson DM, Perman WH. Improved detectability in low SNR MRI by means of a phase-corrected real reconstruction. Med Phys 1989; 16:813–817.
9. Nordell B, Stahlberg F, Ericsson A, Ranta C. A rotating phantom for the study of flow effects in MR imaging. Magn Reson Imaging 1988; 6:695–705.
10. Dixon WT, Du LN, Faul DD, Gado M, Rossnick S. Projection angiograms of blood labeled by adiabatic fast passage. Magn Reson Med 1986; 3:454–462.
11. Maudsley AA. Dynamic range improvements in NMR imaging using phase scrambling. J Magn Reson 1988; 76:287–305.